# On the physics of applying finite width and geometry correction factors in fatigue crack growth predictions of GLARE

Zhao, Yuan; Alderliesten, René; Zhou, Zhengong; Fang, Guodong; Zhang, Jiazhen; Benedictus, Rinze

**DOI**
10.1016/j.ijfatigue.2018.08.021

**Publication date**
2018

**Document Version**
Final published version

**Published in**
International Journal of Fatigue

International Journal of Fatigue 117 (2018) 189–195

Contents lists available at ScienceDirect

International Journal of Fatigue

journal homepage: www.elsevier.com/locate/ijfatigue

# On the physics of applying finite width and geometry correction factors in fatigue crack growth predictions of GLARE

Yuan Zhao[a,b], René Alderliesten[b], Zhengong Zhou[a], Guodong Fang[a,*], Jiazhen Zhang[a], Rinze Benedictus[b]

[a] Science and Technology on Advanced Composites in Special Environments Key Laboratory, Harbin Institute of Technology, Harbin 150001, PR China
[b] Structural Integrity & Composites Group, Faculty of Aerospace Engineering, Delft University of Technology, Kluyverweg 1, 2629 HS Delft, The Netherlands

ARTICLE INFO

*Keywords:*
Fibre metal laminates
Finite width correction
Stress intensity factor
Energy
Fatigue

ABSTRACT

In general, a finite width correction to stress intensity factor (SIF) is required in the fatigue crack growth. The finite width correction factor can be explained physically from the energy point of view. It is assumed that the finite width correction factor primarily constitutes an energy correction factor, i.e. it corrects the applied load for the work applied. To evaluate the finite width correction for FMLs, constant amplitude load fatigue crack growth tests were performed on monolithic aluminium 2024-T3 and the Fibre Metal Laminate GLARE containing 2024-T3 aluminium layers. The loads and displacements were recorded to quantify the total amount of work applied throughout each fatigue test. The crack length and delamination size were monitored by using digital image correlation technique to evaluate the dissipative energy. It appears that the Feddersen's and all other standard finite width correction significantly overestimates the effect for FMLs. The finite width correction to SIF for FMLs is small but cannot be neglected, and it is also greatly related to the Glare grades, stress ratio and stress level.

## 1. Introduction

For many decades, fatigue crack growth is predicted using Linear Elastic Fracture Mechanics (LEFM). In particular the Stress Intensity Factor (SIF) is commonly applied, as originally correlated to the crack growth rate by Paris [1]. It is generally acknowledged that the expression for the SIF must be modified with corrections factors in case finite dimensions are considered [2]. These finite width correction factors are considered scale factors to obtain solutions for finite plates using the expression for infinite plates [3].

As for a through-thickness centre cracked sheet of width $W$, thickness $B$ and crack length $2a$, a tensile force is applied to produce a uniform tensile stress normal to the plane of crack extension. Reviewing the early literature, various corrections have been proposed, with the predominant focus on increasing accuracy in particular for high values of 2a/W [4–15]. Irwin [4] developed a correction that appeared to be valid at most to $2a/W < 0.5$. Isida [5] developed a correction using series expansion, which appeared to be equally accurate as the equation proposed by Feddersen [6]. The excellent correlation between this secant formulation by Feddersen with Isida's correction, has for a while led to the idea that this Feddersen's equation may be in fact exact [7]. However, Koiter [8] demonstrated the exact limit of F(a) for $2a/W \rightarrow 0$, and proposed a formulation which was slightly more accurate than the formulations of Isida and Feddersen, in particular for $2a/W > 0.8$. Several finite width correction schemes proposed by the above authors are listed in Table 1.

Fig. 1 provides the finite width correction factors given in Table 1. It can be observed that the Feddersen's, Koiter's and Isida's curves correlate very well. But the 'secant-formula' of Feddersen's finite width correction factor is the most simple form. In brief, most work aims at the mathematical exercise to develop a closed form solution for the finite width correction in relation to the linear elastic stress field equations, like the ones developed in parallel by respectively Westergaard [10] and Koiter [11]. Recently, the net-section strain energy method proposed by Chandran [15] was used to explain the finite width correction factor. Furthermore, some nonlinear effects due to crack front plastic yield effect and possible small crack extension prior to fracture instability were studied with a nonlinear energy correction [16]. What seems to receive attention to lesser extent is the validity and/or the physical meaning of these linear elastic stress field corrections for the case of crack tip plasticity, in particular large scale plasticity at $2a/W > 0.8$, which invalidates the concept of SIF in LEFM.

As for Fibre Metal Laminates (FMLs), two specific observations in that respect have led to the research discussed in the current paper. The

* Corresponding author.
*E-mail address:* fanggd@hit.edu.cn (G. Fang).

https://doi.org/10.1016/j.ijfatigue.2018.08.021
Received 1 June 2018; Received in revised form 12 July 2018; Accepted 13 August 2018
Available online 16 August 2018
0142-1123/ 

**Table 1**
Overview of the finite width corrections proposed by various authors.

| Year | Author | Correction | Validity | Reference |
|---|---|---|---|---|
| 1959 | Koiter | $F(a)=\frac{1-0.5\frac{2a}{W}+0.326\left(\frac{2a}{W}\right)^2}{\sqrt{1-\frac{2a}{W}}}$ | $0\leqslant\frac{2a}{W}\leqslant 0.8$ | [4] |
| 1960 | Dixon | $F(a)=\frac{1}{\sqrt{1-\left(\frac{2a}{W}\right)^2}}$ | | [9] |
| 1965 | Isida | $F\left(\frac{2a}{W}\right)$, tabular | $0\leqslant\frac{2a}{W}\leqslant 0.8$ | [6,8] |
| 1967 | Feddersen | $F(a)=\frac{1}{\sqrt{\cos\left(\frac{\pi a}{W}\right)}}$ | $0\leqslant\frac{2a}{W}\leqslant 0.8$ | [7] |
| 1967 | Irwin | $F(a)=\frac{1}{\sqrt{\frac{W}{\pi a}\tan\left(\frac{\pi a}{W}\right)}}$ | $0\leqslant\frac{2a}{W}\leqslant 0.5$ | [8] |

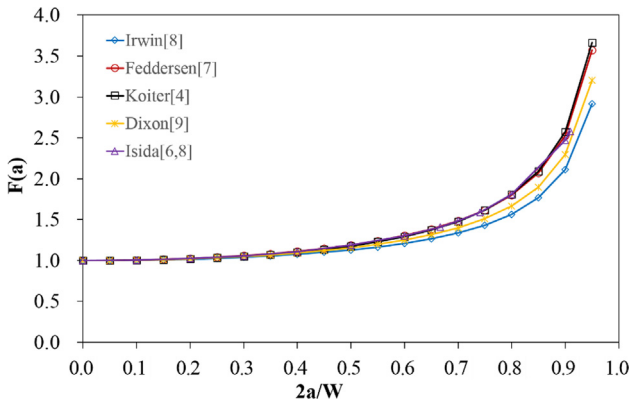


**Fig. 1.** Illustration of finite width correction factors given in Table 1.

first observation relates to the fatigue crack growth prediction methods developed for FMLs [17], in which two distinct SIFs are superimposed; one is the SIF for a centre crack under far field uniaxial loading, and the other the SIF for the bridging stresses at either the crack flank or the delamination contour restraining the crack opening. Both Alderliesten [18] and Wilson [19] observed that the finite width correction factor should not be incorporated in the SIF for the centre crack under far field uniaxial loading. If the Feddersen correction would be applied in that expression, the fatigue crack growth for FMLs would be significantly over-predicted. Leaving the correction out of the expression for this SIF led to only a slight underestimation of the growth. Hence, current crack growth methods for FMLs do not incorporate finite width corrections.

The second observation is more recent, and discussed by Alderliesten [20], where the stress ratio correction for monolithic metals generally attributed to plasticity induced crack closure, is explained to relate mostly to correcting a stress-based method for the physical strain energy dissipation process that fatigue crack growth constitutes. These two observations may be interpreted in the following way. In constant amplitude loading, the change in compliance results in an increase in maximum displacement, which implies that the amount of work applied to the specimen is increasing throughout the test. To capture the effect of this increase, the finite width correction is applied. This change in compliance is smaller for FMLs compared to monolithic metals because of the bridging fibres.

Thus, the hypothesis for the current paper is that the finite width correction primarily corrects for the different amount of work applied to the sample or structure throughout the test. To test this hypothesis, fatigue tests have been performed on both monolithic aluminium panels and Glare laminates.

## 2. Experiments

### 2.1. Materials

Glare as a member of Fibre Metal Laminates [21], consists of alternating layers of thin aluminium 2024-T3 sheets and S2-glass fibres adhesively bonded together in a FM94 adhesive system. A clear coding system was used to identify the Glare grade and lay-up. Glare has six standard grades: Glare 1, Glare2A, Glare2B, Glare3, Glare4A and Glare4B, Glare 5, Glare 6A and Glare 6B, which are respectively corresponding to different prepreg orientations in fibre layer relative to the rolling direction of the aluminium: 0/0, 0/0, 90/90, 0/90, 0/90/0, 90/0/90, 0/90/90/0, +45/−45 and −45/+45 respectively. Each grade has a large amount of lay-ups. For instance, the code Glare 3-5/4-0.4 means respectively the Glare 3 grade, the lay-up with [2024-T3/0 glass fibre/90 glass fibre /2024-T3/0 glass fibre/90 glass fibre/2024-T3/90 glass fibre/0 glass fibre/2024-T3/90 glass fibre/0 glass fibre/2024-T3]. In the present study, the symmetrical Glare laminate lay-ups were used to avoid bending effects from unsymmetrical internal stresses. In this work, materials had Aluminium 2024-T3 panels with thickness 1.2 mm and three kinds of Glare grades.

### 2.2. Test matrix and test procedure

Based on the ASTM E647-15el standard [22], the middle-tension (M(T)) fatigue tests with aluminium and different Glare grades, stress ratio and stress level were conducted to study their effect on the finite width correction factors. The detail geometry dimensions of all fatigue

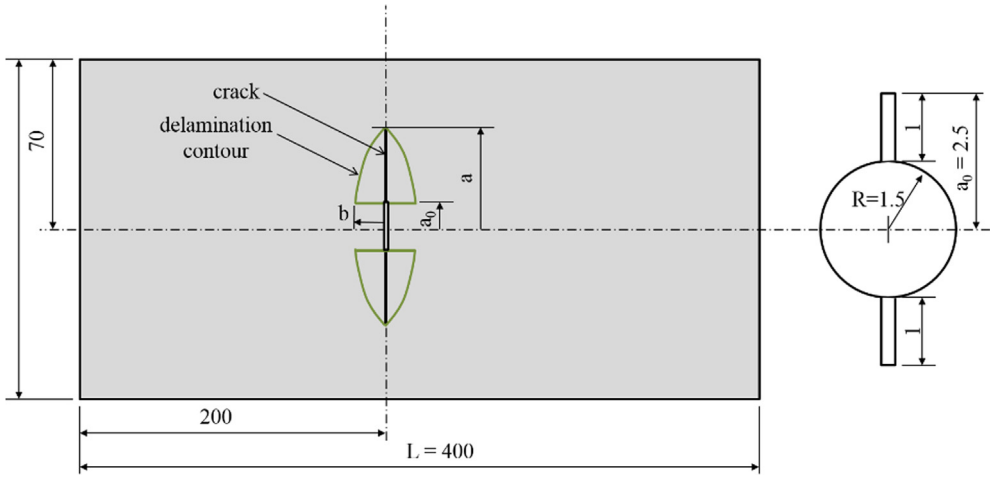


**Fig. 2.** The middle tension (M(T)) specimen (all dimensions in mm) and crack delamination contour during fatigue test.

**Table 2**
Test matrix.

| Material | Maximum stress [MPa] | Stress ratio [–] | Comments |
|---|---|---|---|
| Aluminium 2024-T3 | 100 | 0.05 | Two stress levels and one stress ratio |
| | 60 | 0.05 | |
| Glare 2A-4/3-0.4 | 160 | 0.05 | Four stress levels and two stress ratios |
| | 200 | | |
| | 240 | 0.5 | |
| | 280 | | |
| Glare3-5/4-0.4 | 120 | 0.05 | Four stress levels and two stress ratios |
| | 180 | 0.5 | |
| | 200 | | |
| | 240 | | |
| Glare4B-5/4-0.4 | 100 | 0.05 | Three stress levels and two stress ratios |
| | 120 | | |
| | 180 | 0.5 | |

specimen are shown in Fig. 2. The length and width of the specimen are 400 mm and 140 mm, respectively. To produce a centre crack, a hole with 1.5 mm radius is drilled in the centre of the specimen. Two 1 mm length initial cracks along the width direction are cut from the interior edge of the hole using a jig saw. To illustrate the different factors (Glare grades, stress ratio and stress level), the test matrix in this work is listed in Table 2.

The monolithic Aluminium 2024-T3 panels are used to validate the earlier mentioned finite width corrections. The interior stress in the Aluminium layers in each Glare lay-up can be calculated using the classical laminate theory [23–25]. For the applied stress levels, these stresses are listed in Table 3. It can be observed that the Aluminium stress in Glare 2A-4/3-0.4 under 200 MPa stress and 0.05 stress ratio is similar to that in Glare 3-5/4-0.4 under 180 MPa stress and 0.5 stress ratio. Similarly, Glare 3-5/4-0.4 under 120 MPa stress and 0.05 stress ratio, Glare 2A-4/3-0.4 under 160 MPa stress and 0.05 stress ratio are corresponding to Glare 4B-5/4-0.4 under 100 MPa stress and 0.05 stress ratio, Glare 4B-5/4-0.4 under 120 MPa stress and 0.05 stress ratio, respectively.

All tests were performed using an MTS 250 kN fatigue testing machine at a frequency of 10 Hz in unconditioned ambient lab-air environment. Hence, it should be noted that if the applied stress was small, the testing time extended over day-time and night-time. As a consequence, the diurnal temperature may in some cases influence the testing results, as will be explained later. All tests were performed applying a constant amplitude load spectrum.

### 2.3. Measurement techniques and data evaluation

In order to study the fatigue crack propagation and delamination growth behaviour, the crack length and delamination shapes were recorded during the fatigue test using digital image correlation (DIC) technique, as shown in Fig. 3a. DIC is an innovative, full-field, non-contact optical technique to track the surface displacements of deforming materials. It is based on comparing digital images obtained by CCD cameras at different stages of deformation: one before deformation (known as reference image) and the other one after deformation (known as deformed image) [26–28]. The accuracy of adopting DIC for this purpose has been verified by the chemical etching specimens post-mortem [29]. The principle of observing subsurface delamination shapes by recording surface deformations is based on the difference of strain between delaminated and non-delaminated areas. As for Glare, the metal layers of delaminated areas do not carry any or negligible load, because most of the load is transferred to the fibre layers [30]. Thus, boundaries of delamination region can be clearly distinguished, as demonstrated in Fig. 3b. The delamination area was calculated by integrating the delamination shape. The crack propagation length was obtained by measuring the deformed surface photos. Images were taken with the DIC camera with intervals of which the length was selected based on observed crack growth rate.

**Table 3**
Aluminium stresses in each Glare grades with different applied stresses and stress ratios.

| FMLs | Applied stresses | | Aluminium layer stresses | |
|---|---|---|---|---|
| | Smax [MPa] | R | Smax [MPa] | R |
| Glare2A-4/3-0.4 | 160 | 0.05 | 208.5 | 0.184 |
| | 200 | 0.05 | 253.3 | 0.16 |
| | 240 | 0.5 | 298.2 | 0.56 |
| | 280 | 0.5 | 343 | 0.554 |
| Glare3-5/4-0.4 | 120 | 0.05 | 172 | 0.151 |
| | 180 | 0.5 | 248.9 | 0.543 |
| | 200 | 0.5 | 274.5 | 0.539 |
| | 240 | 0.5 | 325.8 | 0.534 |
| Glare4B-5/4-0.4 | 100 | 0.05 | 167 | 0.157 |
| | 120 | 0.05 | 196.7 | 0.141 |
| | 180 | 0.5 | 285.7 | 0.569 |

If one assumes that the load-displacement curve runs through the origin, then the applied work $U_N$ can be estimated with the maximum loads and displacements measured during the fatigue tests [31]:

$$U_N = \frac{1}{2} P_{\max,N} \delta_{\max,N} \tag{1}$$

where $P_{\max,N}$ is the maximum load applied at the cycle number $N$, $\delta_{\max,N}$ is the maximum displacement at the cycle number $N$. The reader should note that a more accurate estimation of the applied work requires multiple measurements through the load-displacement fatigue cycle.

The original applied work $U_0$ relates to a specimen containing no crack, which cannot be established with the test specimen after the pre-crack has been created. Theoretically, $U_0$ can be calculated using the material's Young's modulus in combination with the specimen dimensions, but it can also be approximated with the data obtained at the first load cycle. Hence for the first load cycle Eq. (1) one obtains:

$$U_0 = \frac{1}{2} P_{\max,0} \delta_{\max,0} \tag{2}$$

where $P_{\max,0}$ is the maximum force at the first cycle, $\delta_{\max,0}$ is the corresponding displacement at the first cycle.

Here, the finite width correction factor can be expressed by

$$F(a) = \frac{U_N}{U_0} \tag{3}$$

In agreement with standard finite width corrections, the $F(a)$ was calculated and then plotted following the $U_N/U_0$ against $2a/W$.

## 3. Results and discussion

### 3.1. Width correction factor for Aluminium 2024-T3

The fatigue tests for Aluminium 2024-T3 with centre crack under maximum stress 100 MPa and 60 MPa were both conducted with a stress ratio of 0.05, as listed in Table 2. The applied load and maximum displacement were recorded to calculate the $F(a)$ using Eqs. (1)–(3). To examine whether the finite width correction is indeed explained by the application of energy, the $F(a) - 2a/W$ curves of Aluminium 2024-T3 obtained from these two fatigue tests are plotted together with traditional finite width correction factors in Fig. 4. It can be observed that the correction factor obtained from the test with maximum stress 100 MPa is in good agreement with the traditional finite width correction factors, but the results obtained from the test with maximum stress 60 MPa deviates from the trend. The finite width correction for Aluminium 2024-T3 under maximum stress 60 MPa drops below 1 to about on average 0.97–0.98.

This deviation is the consequence of estimating the applied work

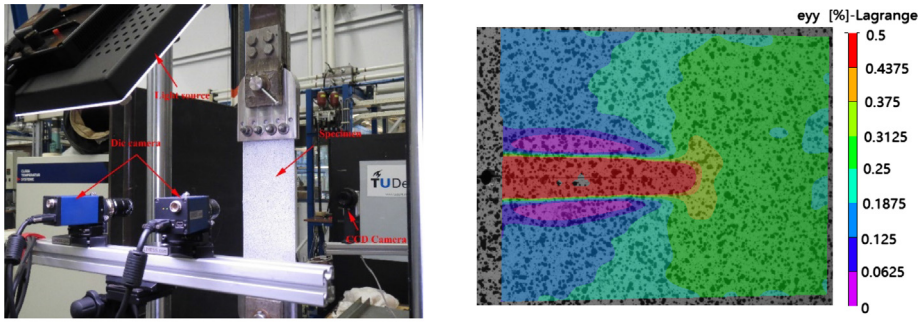


**Fig. 3.** (a) Measurement setup and (b) surface displacement field of Glare specimen.

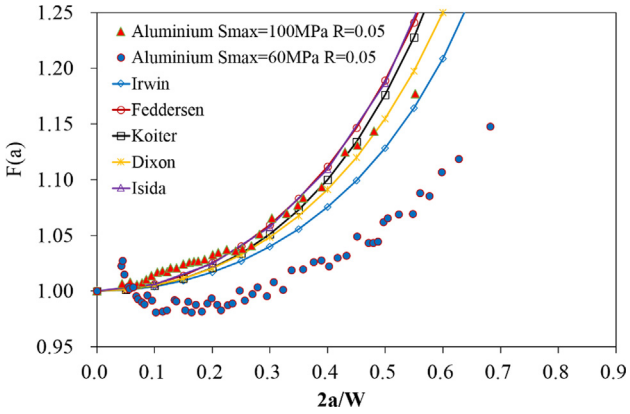


**Fig. 4.** Comparison between correction factor obtained by energy and the standard finite width correction factors without considering thermal deformation.

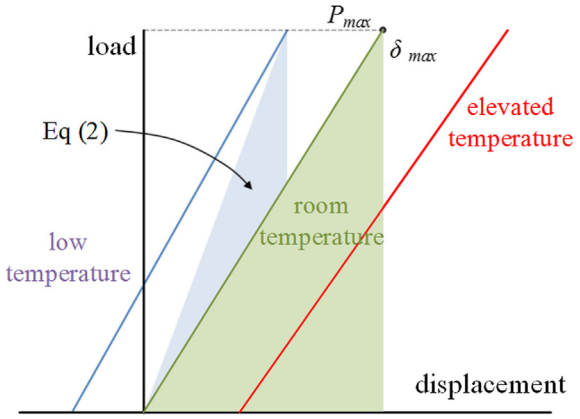


**Fig. 5.** Illustration of the inadequacy of estimating the applied work based on maximum load and displacements only in the case where the ambient temperature changes.

using maximum load and displacement only (assuming the curve through the origin) in combination with the experimental environment. The fatigue test of the specimen under maximum stress of 60 MPa took many hours, which implies running overnight. Throughout the test, the ambient temperature was not controlled with the consequence that it dropped a few degrees overnight. The stiffness of the specimen changes with the ambient temperature following the coefficient of thermal expansion and the dependency of the material's Young's modulus on temperature. Under force-controlled conditions, this imposes the load-displacement curve to move left with a slightly increased slope, as illustrated in Fig. 5. Theoretically, the work applied remains the area underneath the load-displacement curve, implying that the work is only affected by the change in Young's modulus. However, here only maximum load and displacement were used, assuming that the load displacement curve went through the origin. As Fig. 5 illustrates, this introduces the influence of thermal expansion. For Aluminium 2024-T3, the coefficient of thermal expansion α and elastic modulus are $23.2{\cdot}10^{-6}$ m/m/°C and 73 GPa, respectively. The theoretically applied work on the uncracked Aluminium panel follows from Eq. (1):

$$U_0 = \frac{1}{2}P_{\max,0}\delta_{\max,0} = \frac{1}{2}AL\frac{\sigma^2_{\max,0}}{E} = \frac{60^2}{2\times 73000}AL = 2.4658{\cdot}10^{-2}\times AL(\text{N}{\cdot}\text{mm}) \quad (4)$$

where $A$ and $L$ are the cross-section and length of specimen, respectively. If the temperature reduces with for example 2 °C at night, Eq. (2) effectively becomes

$$U'_0 = \frac{1}{2}P_{\max,0}\delta_{\max,0} = \frac{1}{2}AL\sigma_{\max,0}\left(\frac{\sigma_{\max,0}}{E}-\alpha\Delta T\right) = \frac{AL}{2}\times 60\times\left(\frac{60}{73000}-23.2{\cdot}10^{-6}\times 2\right)^2 AL = 2.3268{\cdot}10^{-2}\times AL(\text{N}{\cdot}\text{mm}) \quad (5)$$

where, $\alpha$ is the coefficient of thermal expansion, $\Delta T$ is the diurnal temperature. Then Eq. (3) yields $F(a) = U'_0/U_0 = 2.3268{\cdot}10^{-2}/2.4658{\cdot}10^{-2} = 0.94$, which is below 1. In reality, the correction data should be calculated based on the actual stiffness without the effect of the coefficient of thermal expansion. Thus, the environmental temperature has an effect on the finite width correction, through its effect on the material's Young's modulus. To eliminate this effect, it is better to control the environmental temperature, and keep it unchanged during fatigue tests.

### 3.2. Evaluation of finite width correction for Glare with different grades

Fig. 6 illustrates the finite width corrections according to Eq. (3) for Glare with different grades based on the maximum applied work. It can be observed in Fig. 6 that the finite width corrections are greatly different for the different Glares under different maximum stress and stress ratios. The correction factors change with crack propagation ratio (from 2a/W is 0.0 to 0.8) from about 1 to 1.175, as shown in Fig. 6(a), which is a relative small correction in comparison to the standard finite width correction. The Glare finite width corrections increase slower with the crack length, not asymptotically up to infinite, but to a finite value for 2a/W = 1. When 2a/W = 1, it is assumed that all metal layers are cracked and that the laminate stiffness is defined by intact fibres layers only. Therefore the width correction factor $F(a)$ for 2a/W = 1 is expressed as:

$$F(a) = \frac{U_f}{U_0} \quad (6)$$

where $U_f$ and $U_0$ are the maximum possible applied work for 2a/W = 1 and the original applied work. In theory, $U_f$ and $U_0$ can be calculated using the material's Young's modulus in combination with the specimen

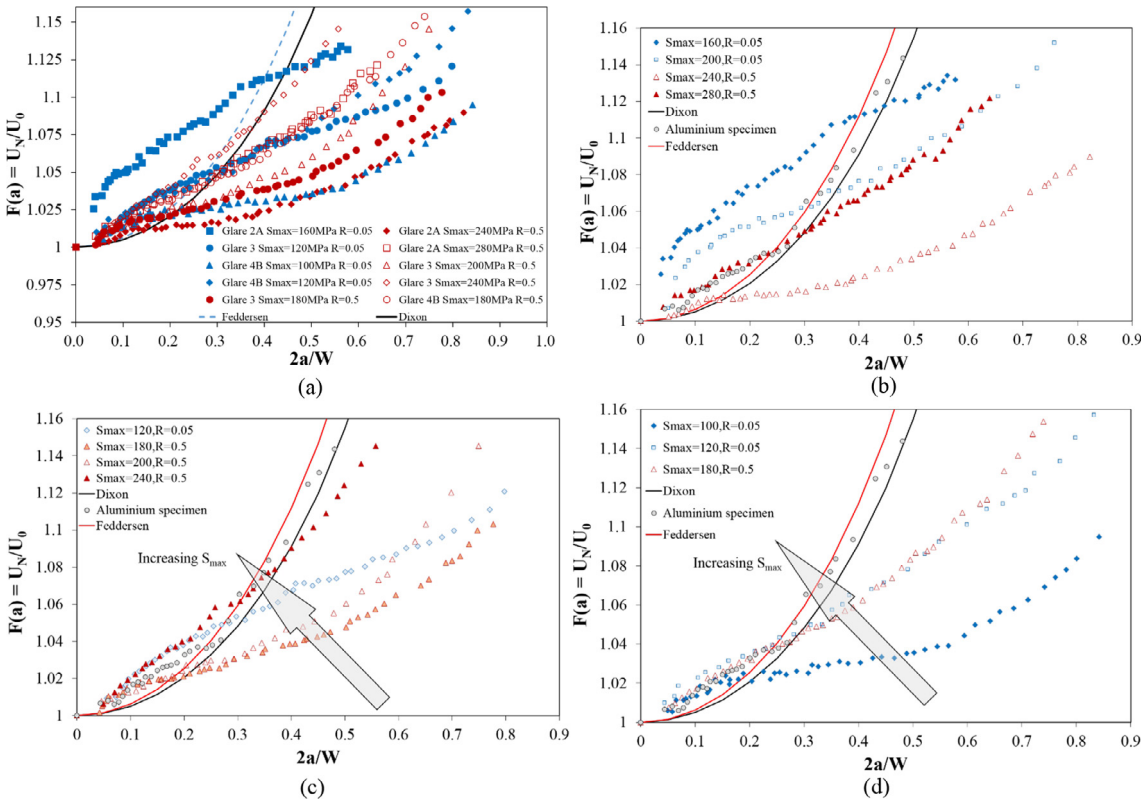


**Fig. 6.** $F(a)-a/W$ curves for different Glares: (a) all Glares, (b) Glare 2A, (c) Glare 3, (d) Glare 4B.

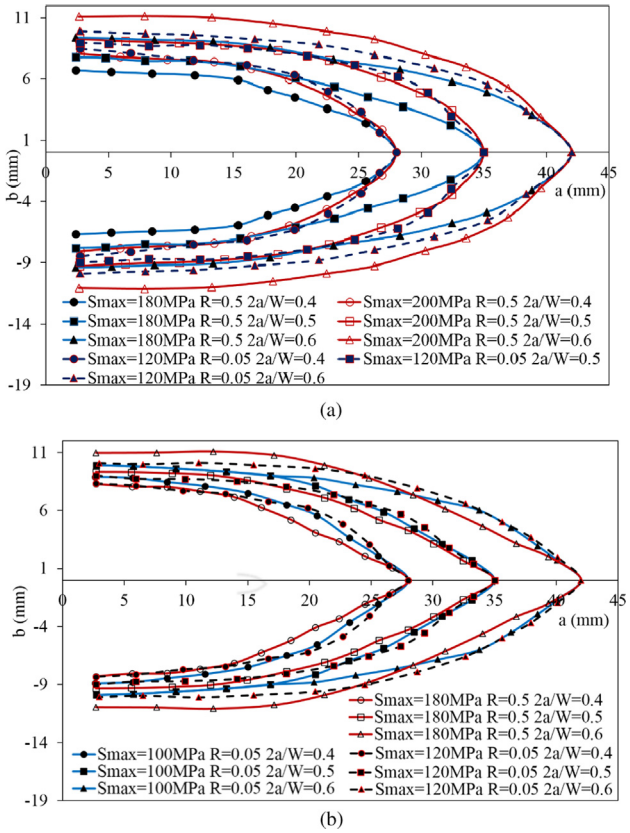


**Fig. 7.** Delamination shapes corresponding to 2a/W = 0.4, 0.5 and 0.6 for (a) Glare 3, and (b) Glare 4B.

dimensions as following:

$$U_f = \frac{1}{2}\frac{\sigma_{eff}^2}{E_f} \tag{7}$$

$$U_0 = \frac{1}{2}\frac{\sigma_{appl}^2}{E_{lam}} \tag{8}$$

where $\sigma_{eff}$ and $\sigma_{appl}$ are the effective stress and applied stress respectively, $E_f$ and $E_{lam}$ are the Young's modulus for intact fibre layers and laminate. Writing $\sigma_{eff}$ and $\sigma_{appl}$ in terms of load,

$$\sigma_{eff} = \frac{P_{\max,0}}{W \cdot t_f} \tag{9}$$

$$\sigma_{appl} = \frac{P_{\max,0}}{W \cdot t_{lam}} \tag{10}$$

where $t_f$ is the total thickness of intact fibre layers and $t_{lam}$ is the thickness of laminate. Hence, on the basic of Eqs. (7)-(10), Eq. (6) becomes,

$$F(a) = \frac{E_{lam}}{E_f} \cdot \left(\frac{t_{lam}}{t_f}\right)^2 \tag{11}$$

Eq. (11) is the finite value for 2a/W = 1. It can be observed that for each Glare grade, the finite values for 2a/W = 1 are different.

Fig. 6(b)–(d) are the individual finite width corrections for Glare 2A, Glare 3 and Glare 4B, respectively. It can be observed in Fig. 6(c) and (d) that the higher the maximum applied stress, the closer the curves move towards the standard finite width correction. This trend seems less clear for Glare 2A compared to the other two, which can be attributed to the higher laminate stiffness. The noise in the displacement measurements is higher for stiffer laminates, because the displacements are lower. It can be observed in Fig. 6(b) that the $F(a)-a/W$ curve for Glare 2A with a relative small maximum stress 160 MPa greatly deviated from the origin of the correction data. As for the Glare 2A with

maximum stress 240 MPa and 280 MPa, the noise in the displacement becomes small, and the obtained results are good.

The delamination shapes of Glare 3 and Glare 4B at equal crack length corresponding to 2a/W = 0.4, 0.5 or 0.6 are shown in Fig. 7. As for the same stress ratio, different maximum stresses for Glare 3 or Glare 4B have similar delamination shapes as shown in Fig. 7(a) and (b). But with different stress ratio, the delamination shapes for Glare 3 and Glare4B are different. When the maximum stress applied on Glare does not have a great difference, the vertical delamination width close to the crack tip for R = 0.05 is larger than that for R = 0.5. Thus, the delamination area for R = 0.05 is bigger than for R = 0.5 when the crack length is same and the maximum stress applied on the Glare is little difference. The far field stress in the Aluminium layer will increase with the increase of delamination area. Then, the finite width correction factor will increase as well. Both Glare 3 and Glare 4B at the same stress ratio, the delamination area increases with increase of the maximum stress. It also can be seen in Fig. 7 that with the increase of crack length, the delamination length in the horizontal and vertical directions $a_0$ and $b_0$ also increase, but to a different extent. It can be observed that the stiffer the laminate is, the more noise in the results, yielding not always clear curves. At equal crack length, the delamination for lower stress ratio is larger, which means a higher specimen compliance. Hence, the force-displacement of Glare becomes less steep when larger delamination are present, which brings it closer to the standard correction.

The $F(a)-a/W$ curves and delamination shape for different Glare grades under same stress ratios and with similar far field stress in Aluminium layer also can be examined as shown in Figs. 8 and 9. The far field stress and stress ratio in the Aluminium layers of Glare 3 under 200 MPa R = 0.5 are 274.5 MPa and 0.539, which are similar with

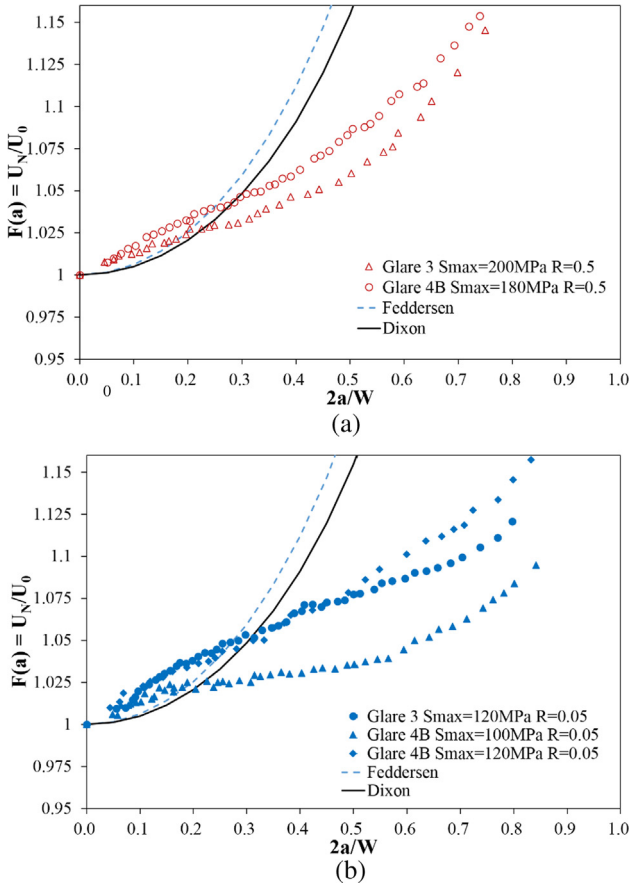


**Fig. 8.** $F(a)-a/W$ curves for different Glares with similar far field stress in the aluminium layer: (a) R = 0.5 and (b) R = 0.05.

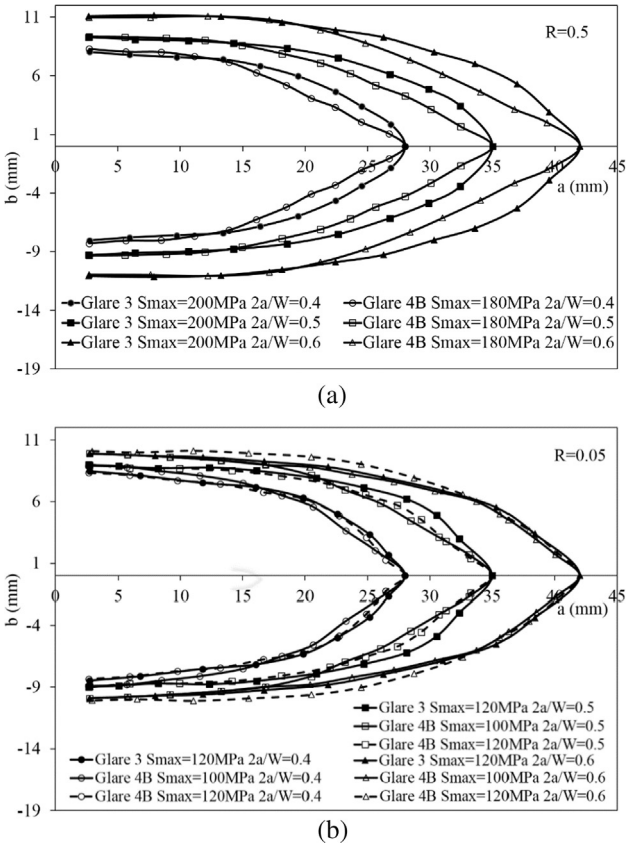


**Fig. 9.** Delamination shape for different Glares with similar far field stress in the aluminium layer corresponding to 2a/W = 0.4, 0.5 and 0.6, (a) R = 0.5 and (b) R = 0.05.

285.7 MPa and 0.569 for Glare 4B under 180 MPa and R = 0.5, as listed in Table 3. The $F(a)-a/W$ curves and delamination shape for Glare 3 and Glare 4B under R = 0.5 are shown in Figs. 8(a) and 9(a). It can be observed that Glare 3 under 200 MPa, R = 0.5 and Glare 4B under 180 MPa, R = 0.5 have similar correction curves, because the delamination shapes were similar.

Similarly, the far field stress and stress ratio in Aluminium layer of Glare 3 under 120 MPa R = 0.05 similar with Glare 4B under 100 MPa R = 0.05 and Glare 4B under 120 MPa R = 0.05 as listed in Table 3. However, the difference between Glare 4B under maximum 120 MPa R = 0.05 and Glare 4B under maximum 100 MPa R = 0.05 is apparent. Purely based on the delamination shapes shown in Fig. 9(b), one would expect the F(a) for Glare4B at 100 MPa to be close to the curves of Glare3 and Glare4B at 120 MPa. However, great extent of the difference seen in Fig. 8(b), may be attributed to the fact that the test on Glare4B at 100 MPa, run over night as well, yielding similar temperature influences as the monolithic aluminium specimen tested at 60 MPa.

It can be seen in Fig. 8(b) that the $F(a)-a/W$ curve for Glare 4B under maximum 120 MPa R = 0.05 is gradually higher than that for Glare 3 under maximum 120 MPa R = 0.05. As for 2a/W = 0.4 and 0.5, the delamination area for Glare 3 under maximum 120 MPa R = 0.05 is larger than that of Glare 4B under maximum 120 MPa R = 0.05. The phenomenon is contrary when 2a/W equals to 0.6 as shown in Fig. 9(b). The change of delamination is in agreement with the change trend of $F(a)-a/W$ curve for Glare 4B under maximum 120 MPa R = 0.05 and Glare 3 under maximum 120 MPa R = 0.05.

## 4. Conclusions

The finite width correction factor can be interpreted as the correction to the applied work to the specimen in case of constant amplitude

loading, which is briefly validated with data obtained from monolithic aluminium. As for Glare, the finite width correction factor obtained from the applied work is significantly smaller than that of standard finite width corrections. The standard finite width corrections, such as Feddersen's and Dixon's correction, are inappropriate for FMLs. The maximum stress, stress ratio and Glare grades all influence the finite width correction factor for different Glares, mostly through the effective size of the delaminations generated. Generally, the finite width correction factor is moving towards the standard finite width correction factor with the increase of maximum stress. This change of finite width correction factor is related to the delamination area between fibre layers and aluminium layers, which is influenced by maximum applied stress, stress ratio and Glare grades.

The one fatigue test on aluminium that deviated from the standard finite width correction illustrated the effect of environment on the finite width correction factor. Although in the current study this factor was insufficiently based on the applied work calculated with maximum load and displacement, this deviation does reveal that ambient temperature variations do impose scatter to the data, when it is not accounted for with standard finite width corrections. The relationship between temperature and finite width correction factor will be further studied in the future.

## Acknowledgement

Support for this work by the State Scholarship Fund from the China Scholarship Council (CSC), National Natural Science Foundation of China (Grant Nos. 11572101, 11672089) and National Key Basic Research Program of China (2014CB046505).

## References

[1] Paris PC, Gomez MP, Anderson WE. A rational analytic theory of fatigue. Trends Eng 1961;13:9–14.
[2] Wang WD, Rans C, Zhang ZN, Benedictus R. Prediction methodology for fatigue crack growth behaviour in Fibre Metal Laminates subjected to tension and pin loading. Compos Struct 2017;182:176–82.
[3] Brown WFJ, Srawley JE. Plane strain crack toughness testing of high-strength metallic materials. Am Soc Test Mater 1966:410.
[4] Irwin GR. Analysis of stresses and strains near the end of a crack traversing a plate. J Appl Mech 1957;24:361–4.
[5] Isida M. Crack tip stress intensity factors for the tension of an eccentrically cracked strip. Lehigh University, Department of Mechanics Report; 1965.
[6] Feddersen C. Discussion to: plane strain crack toughness testing. Am Soc Test Mater 1967:410.
[7] Irwin GR, Liebowitz H, Paris P. A mystery of fracture mechanics. Eng Fract Mech 1968;1:235–6.
[8] Koiter WT. Note on the stress intensity factors for sheet strips with cracks under tensile loads. Delft Technological University, Department of Mechanical Engineering; 1965, Report No. 314.
[9] Dixon JR. Stress distribution around a central crack in a plate loaded in tension: effect of finite width of plate. J Royal Aeronautical Soc 1960;64:141–5.
[10] Westergaard HM. Bearing pressures through a slightly waved surface or through a nearly flat part of a cylinder, and related problems of cracks. J Appl Mech 1939;61:49–53.
[11] Koiter WT. An infinite row of collinear cracks in an infinite elastic sheet. Ingenieur-Archiv 1959;28(1):168–72.
[12] Bowie OL, Neal DM. A note on the central crack in a uniformly stress strip. Eng Fract Mech 1970;2:181–2.
[13] Rooke DP. Width corrections in fracture mechanics. Eng Fract Mech 1970;1:727–8.
[14] Tada H. A note on the finite width corrections to the stress intensity factor. Eng Fract Mech 1971;3:345–7.
[15] Ravi KS. Chandran. Insight on physical meaning of finite-width-correction factors in stress intensity factor (K) solutions of fracture mechanics. Eng Fract Mech 2017;186:399–409.
[16] Liebowitz H, Eftis J. Correcting for nonlinear effects in fracture toughness testing. Nucl Eng Des 1972;18(3):457–67.
[17] Alderliesten RC. The explanation of stress ratio effect and crack opening corrections for fatigue crack growth in metallic materials. Adv Mater Res 2014;891–892:289–94.
[18] Alderliesten RC. How proper similitude could improve our understanding of crack closure and plasticity in fatigue. Int J Fatigue 2016;82:263–73.
[19] Wilson GS. Fatigue crack growth prediction for generalized fiber metal laminates and hybrid materials PhD thesis Delft: Delft University of Technology; 2013.
[20] Alderliesten RC. How proper similitude principles could have improved our understanding about fatigue damage growth. In: Proceedings of the 28th ICAF symposium – Helsinki, 3–5 June 2015.
[21] Vlot A, Gunnink JW. Fibre metal laminates, an introduction. Dordrecht, The Netherlands: Kluwer Academic Publishers; 2001.
[22] ASTM -15e1. Standard test method for measurement of fatigue crack growth rates. American Society for Materials and Testing, ASTM International, 2015. West Conshohocken, USA. p. 1–49. doi: 10.1520/E0647-15E01.
[23] Homan JJ. Fatigue initiation in fibre metal laminates. Int J Fatigue 2006;28:366–74.
[24] Spronk SWF, Sen I, Alderliesten RC. Predicting fatigue crack initiation in fibre metal laminates based on metal fatigue test data. Int J Fatigue 2017;70:428–39.
[25] Alderliesten RC. Fatigue and fracture of fibre metal laminates. Switzerland: Springer International Publishing AG; 2017.
[26] Sutton MA, McNeil SR, Helm JD, Chao YD. Advances in two-dimensional and three-dimensional computer vision. Top Appl Phys 2000;77:323–72.
[27] Lemmen HJK, Alderliesten RC, Benedictus R, Hofstede JCJ, Rodi R. The power of digital image correlation for detailed elastic-plastic strain measurements. In: EMESEG'08 conference, Crete Island, Greece; 2008. p. 73–89.
[28] Corr D, Accardi M, Graham-Brady L, Shah S. Digital image correlation analysis of interfacial debonding properties and fracture behavior in concrete. Eng Fract Mech 2007;74:109–21.
[29] Huang Y, Liu JZ, Huang X, Zhang JZ, Yue GQ. Delamination and fatigue crack growth behaviour in Fiber Metal Laminates (Glare) under single overloads. Int J Fatigue 2015;78:53–60.
[30] S. KHAN. Fatigue crack & delamination growth in fibre metal laminates under variable amplitude loading. Ph.D. thesis. Delft: Delft University of Technology; 2013.
[31] Yao LJ, Alderliesten RC, Zhao MY, R.. Benedictus. Discussion on the use of the strain energy release rate for fatigue delamination characterization. Compos A 2014;66:65–72.